AGU PUBLICATIONS

Geophysical Research Letters

RESEARCH LETTER
10.1002/2016GL070500

Key Points:
- Pine Island Glacier speed is correlated with ocean temperature
- Grounded ice speed slowed by only ~1% despite ~60% drop in ocean heat content
- Ice speed recovered after the cold-ocean anomaly ended

Supporting Information:
- Supporting Information S1
- Movie S1

Correspondence to:
K. Christianson,
knut@uw.edu

Citation:
Christianson, K., et al. (2016), Sensitivity of Pine Island Glacier to observed ocean forcing, *Geophys. Res. Lett.*, *43*, 10,817–10,825, doi:10.1002/2016GL070500.

Received 18 JUL 2016
Accepted 11 OCT 2016
Accepted article online 12 OCT 2016
Published online 30 OCT 2016

Sensitivity of Pine Island Glacier to observed ocean forcing

Knut Christianson[1], Mitchell Bushuk[2,3], Pierre Dutrieux[4,5], Byron R. Parizek[6,7], Ian R. Joughin[4], Richard B. Alley[7], David E. Shean[1,4], E. Povl Abrahamsen[8], Sridhar Anandakrishnan[7], Karen J. Heywood[9], Tae-Wan Kim[10], Sang Hoon Lee[10], Keith Nicholls[8], Tim Stanton[11], Martin Truffer[12], Benjamin G. M. Webber[9], Adrian Jenkins[8], Stan Jacobs[5], Robert Bindschadler[13], and David M. Holland[2]

[1]Department of Earth and Space Sciences, University of Washington, Seattle, Washington, USA, [2]Courant Institute of Mathematical Sciences, New York University, New York, New York, USA, [3]Geophysical Fluid Dynamics Laboratory, Princeton University, Princeton, New Jersey, USA, [4]Polar Science Center, Applied Physics Laboratory, University of Washington, Seattle, Washington, USA, [5]Lamont-Doherty Earth Observatory, Columbia University, Palisades, New York, USA, [6]Mathematics and Geoscience, Pennsylvania State University, DuBois, Pennsylvania, USA, [7]Department of Geosciences and Earth and Environmental Systems Institute, Pennsylvania State University, University Park, Pennsylvania, USA, [8]British Antarctic Survey, Natural Environment Research Council, Cambridge, UK, [9]Centre for Ocean and Atmospheric Sciences, School of Environmental Sciences, University of East Anglia, Norwich, UK, [10]Korea Polar Research Institute, Incheon, South Korea, [11]Department of Oceanography, U.S. Naval Postgraduate School, Monterey, California, USA, [12]Geophysical Institute, University of Alaska Fairbanks, Fairbanks, Alaska, USA, [13]NASA Goddard Space Flight Center, Greenbelt, Maryland, USA

Abstract We present subannual observations (2009–2014) of a major West Antarctic glacier (Pine Island Glacier) and the neighboring ocean. Ongoing glacier retreat and accelerated ice flow were likely triggered a few decades ago by increased ocean-induced thinning, which may have initiated marine ice sheet instability. Following a subsequent 60% drop in ocean heat content from early 2012 to late 2013, ice flow slowed, but by $< 4\%$, with flow recovering as the ocean warmed to prior temperatures. During this cold-ocean period, the evolving glacier-bed/ice shelf system was also in a geometry favorable to stabilization. However, despite a minor, temporary decrease in ice discharge, the basin-wide thinning signal did not change. Thus, as predicted by theory, once marine ice sheet instability is underway, a single transient high-amplitude ocean cooling has only a relatively minor effect on ice flow. The long-term effects of ocean temperature variability on ice flow, however, are not yet known.

1. Introduction

Ice sheets resting on beds below sea level that deepen toward the ice sheet interior are susceptible to marine ice sheet instability [*Mercer*, 1968; *Weertman*, 1974; *Schoof*, 2007]. Flow speed at the grounding line (the transition from grounded to floating ice) increases with ice thickness. Thus, initial grounding line retreat down a sloping bed into thicker ice causes additional ice discharge, thinning, and retreat: a positive feedback [*Weertman*, 1974; *Schoof*, 2007]. For at least the last two decades, ocean-induced melting [*Jacobs et al.*, 1996; *Payne et al.*, 2004; *Jenkins et al.*, 2010; *Jacobs et al.*, 2011; *Dutrieux et al.*, 2014a] has thinned floating ice shelves in West Antarctica's Amundsen Sea Embayment [*Pritchard et al.*, 2012; *Paolo et al.*, 2015], initiating widespread grounding line retreat [*E. J. Rignot*, 1998; *Rignot et al.*, 2014] and increasing discharge [*Mouginot et al.*, 2014]. Models projecting these changes forward often [*Favier et al.*, 2014; *Joughin et al.*, 2014; *Cornford et al.*, 2015], but not always [*Joughin et al.*, 2010; *Parizek et al.*, 2013; *DeConto and Pollard*, 2016], yield eventual ice sheet collapse. Simultaneous observations of the ice sheet and adjacent ocean remain scarce, so that observational validation of model simulations is rare. Here we present the first concurrent multiyear (2009–2014) observations of Pine Island Glacier (PIG), its ice shelf, and the adjacent Amundsen Sea.

From 1974 to 2010, PIG accelerated ~75% to ~4000 m yr^{-1} (Figure 1), increasing its mass imbalance ~750% (from -6.0 ± 6.4 Gt yr^{-1} to -46.1 ± 7.1 Gt yr^{-1}), making PIG the largest single glaciological contributor to global sea level rise (~4%; ~0.11 mm yr^{-1}) [*Joughin et al.*, 2003; *Rignot*, 2008; *Medley et al.*, 2014]. The grounding line retreated concurrently, by as much as 30 km along the ice stream centerline since 1992 [*E. J. Rignot*, 1998; *Rignot et al.*, 2014]. Recent observations and modeling suggest PIG's mass loss was triggered before the satellite era by increased basal melting from greater supply of warm water to the ice shelf base, particularly in

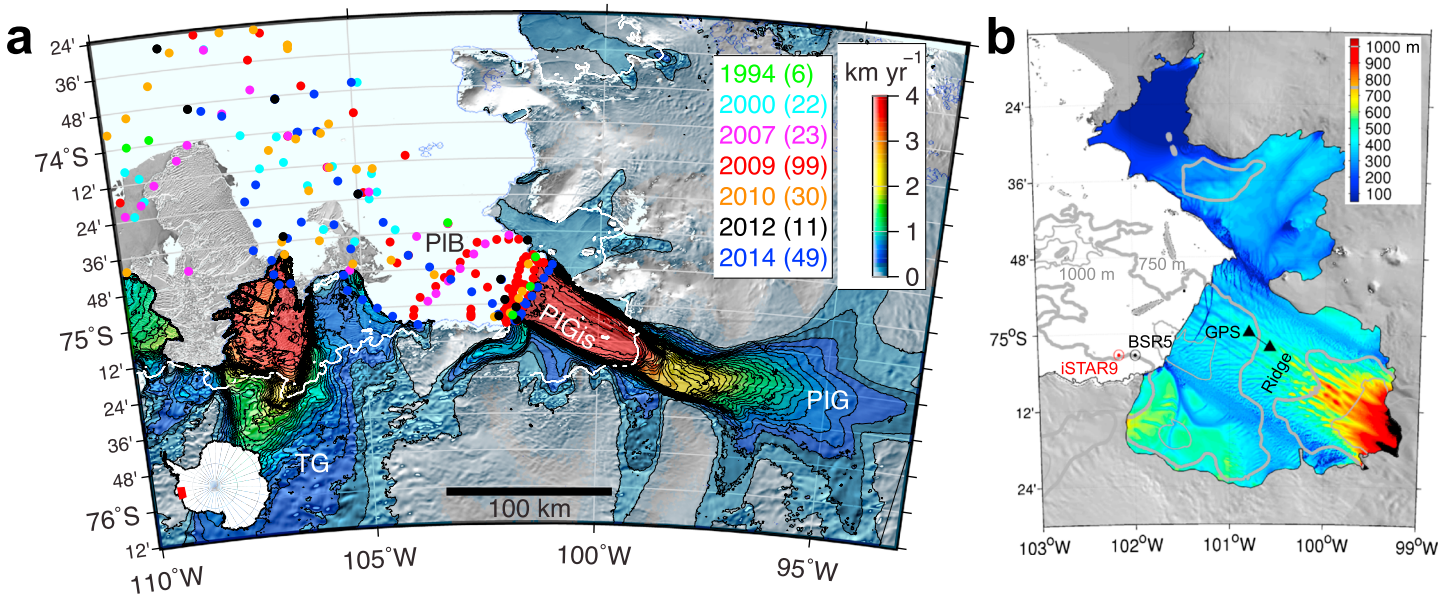

Figure 1. Pine Island Glacier glaciological and oceanographic setting. (a) Ice speed [*Rignot et al.*, 2011a, 2011b] (100 m yr^{-1} contour interval) in the vicinity of Pine Island Glacier plotted over Moderate Resolution Imaging Spectroradiometer (MODIS) image mosaic [*Haran et al.*, 2014]. Pine Island Glacier (PIG), Pine Island Glacier ice shelf (PIGis), Pine Island Bay (PIB), and Thwaites Glacier (TG) are labeled. Locations (and number) of conductivity, temperature, and depth (CTD) casts used to create averaged temperature profiles in Figure 2b are plotted. White line indicates the most recent comprehensively mapped grounding line (2011) [*Rignot et al.*, 2014]. Inset shows map extent in Antarctica. (b) Pine Island Glacier ice shelf draft calculated from a surface digital elevation model derived from Worldview satellite stereoscopic optical imagery [*Moratto et al.*, 2010; *Shean et al.*, 2016] assuming hydrostatic equilibrium. The inversion domain is chosen to be the approximate maximum extent of floating ice (2009–2014). Locations of the ocean moorings (iSTAR9 and BSR5) and GPS sites are shown by circles and a triangle, respectively. The line between triangles indicates extent of GPS site motion. Light gray contours indicate bed elevation. The −750 m bed elevation contour (heavy gray) marks a large bathymetric ridge [*Jenkins et al.*, 2010; *Muto et al.*, 2016] that is oriented transverse to ice flow.

deep regions near the grounding line [*Jacobs et al.*, 1996; *Payne et al.*, 2004; *Jenkins et al.*, 2010; *Joughin et al.*, 2010; *Jacobs et al.*, 2011; *Pritchard et al.*, 2012; *Parizek et al.*, 2013; *Dutrieux et al.*, 2014a; *Favier et al.*, 2014; *Joughin et al.*, 2014; *Mouginot et al.*, 2014; *Cornford et al.*, 2015; *DeConto and Pollard*, 2016]. The resulting thinning reduced drag from local grounding on bed highs and along shear margins, allowing faster flow of the ice shelf and the proximal grounded ice stream feeding it. This speedup led to retreat of the grounding line into deeper water toward the continent and loss of traction where the ice went afloat, a feedback that produced greater thinning, flotation, and grounding line retreat, which continued through 2009 [*E. J. Rignot*, 1998; *Joughin et al.*, 2003; *Rignot*, 2008; *Mouginot et al.*, 2014; *Rignot et al.*, 2014]. Observations and modeling, however, suggest that oceanic forcing varied on multiple timescales in Pine Island Bay during the 1992–2009 retreat [*Thoma et al.*, 2008; *Dutrieux et al.*, 2014a; *St-Laurent et al.*, 2015], likely causing a twofold variation of ocean heat content in the ice shelf cavity [*Dutrieux et al.*, 2014a]. Ice velocity was poorly sampled in time, making it difficult to determine glacier sensitivity to this ocean variability, as, in addition to ocean forcing, ice shelf melt rates are affected by the evolving ice shelf cavity geometry. Model projections of PIG's behavior during the 21st century vary, from sustained but moderate retreat [*Joughin et al.*, 2010] to unstable retreat [*Favier et al.*, 2014], pointing to inadequate process understanding and demonstrating the importance of constraints provided by joint glacier-ocean observations.

To better understand glacier response to ocean forcing, we instrumented the PIG ice shelf and cavity. Ocean moorings have recorded temperature near the ice shelf front since 2009 (Figures 2 and S1 in the supporting information). A Global Positioning System (GPS) array on the PIG ice shelf from January 2012 to January 2014 (Figures 1, 2a, and S2–S3) provided point velocities with high temporal resolution. These data are complemented by velocities and grounding line positions from satellite synthetic aperture radar (SAR) data acquired 13 times from 2009 to 2015 (Figure 3 and Movie S1). Shorter time series of basal-melt rate and ocean properties were also obtained directly from the ice shelf cavity [*Stanton et al.*, 2013]. Together, these data sets reveal the ice flow response to a large (>1°C), prolonged (>1 year) fluctuation in ocean temperature.

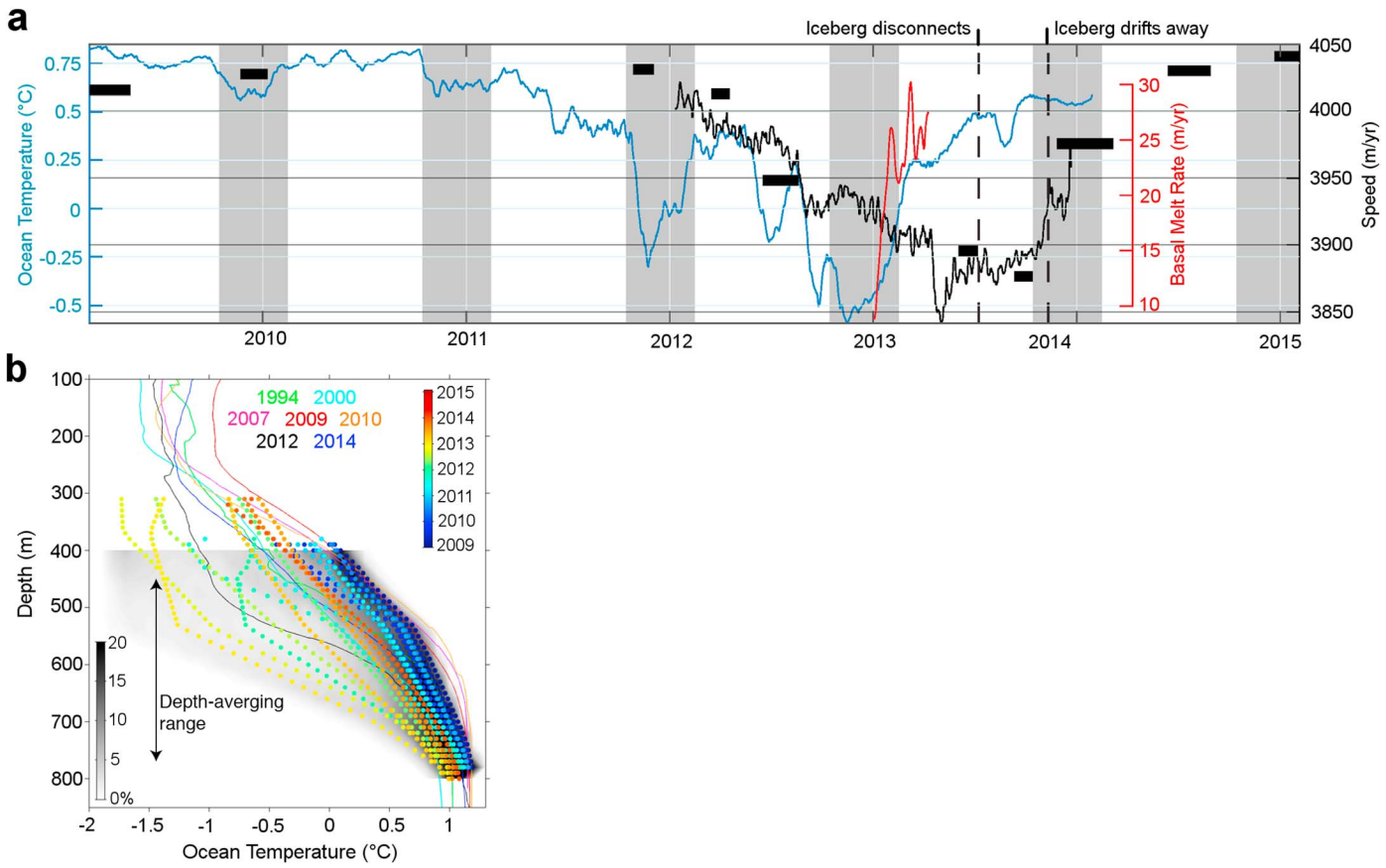

Figure 2. Glacier speed, ocean temperature, and basal-melt rate. (a) Time series of ocean temperature (blue; depth averaged between 450 and 770 m, 30 day moving average), ice speed from GPS (black line) and SAR data (black bars mark time span of individual TerraSAR-X mosaics), and basal-melt rate in vicinity of GPS site (red). Black dashed vertical lines mark dates of iceberg calving and drift away from the coast into Pine Island Bay. Gray bars mark annual ocean temperature minimums (mid-October to mid-February). (b) Ocean temperature between 2009 and 2014 from moored observations (dotted lines) near the Pine Island Glacier ice front and summer CTD casts in Pine Island Bay (solid lines; casts are averaged per cruise, see color code and number of casts in Figure 1a). Shading indicates amount of time (%) spent at a given temperature from the mooring data (2009–2014). Mooring data are colored by date (separate scale from CTD casts).

2. Data and Methods

2.1. GPS Velocities

We deployed five GPS receivers in a strain net around an ice shelf channel (Figure S2). GPS data were collected using dual-frequency receivers (Trimble NetR9 receivers with Trimble Zephyr Geodetic 2 antennas) and processed using differential carrier phase positioning as implemented in the Track software [*Chen*, 1998] relative to a fixed rock site approximately 60 km away (Backer Island) with epoch-by-epoch zenith tropospheric delay estimation [*King*, 2004]. Geodetic positions (relative to WGS84 ellipsoid) were calculated every 30 s. Uncertainties on each position are less than 5 cm in all dimensions. Daily-averaged positions of the Backer Island base station were calculated using GAMIT and stabilized relative to a fixed circum-Antarctic reference frame using a Kalman filter (GLOBK). Geodetic solutions were transformed to a polar stereographic coordinate system (EPSG:3031). Epoch-by-epoch component velocities were derived from 3 day fourth-order polynomial fits to the polar stereographic coordinates (EPSG:3031) calculated using Savitsky-Golay filters [*Press et al*., 2007] and included a scaling factor to account for distance distortion caused by projection. We compared these velocities with velocities derived using several other methods, including those calculated from geodetic coordinates using both epoch-by-epoch coordinates after 3 day fourth-order Savisky-Golay smoothing and daily average coordinates calculated via a standard moving average boxcar window. We also fit over various time windows (6 h, 12 h, 1 day, 3 day, and 1 week). For a given window size, Savitsky-Golay (digital smoothing polynomial) filters will better preserve the higher moments in the original data but retain more noise. However, the long-term velocity trends of interest here (fortnightly or longer) are

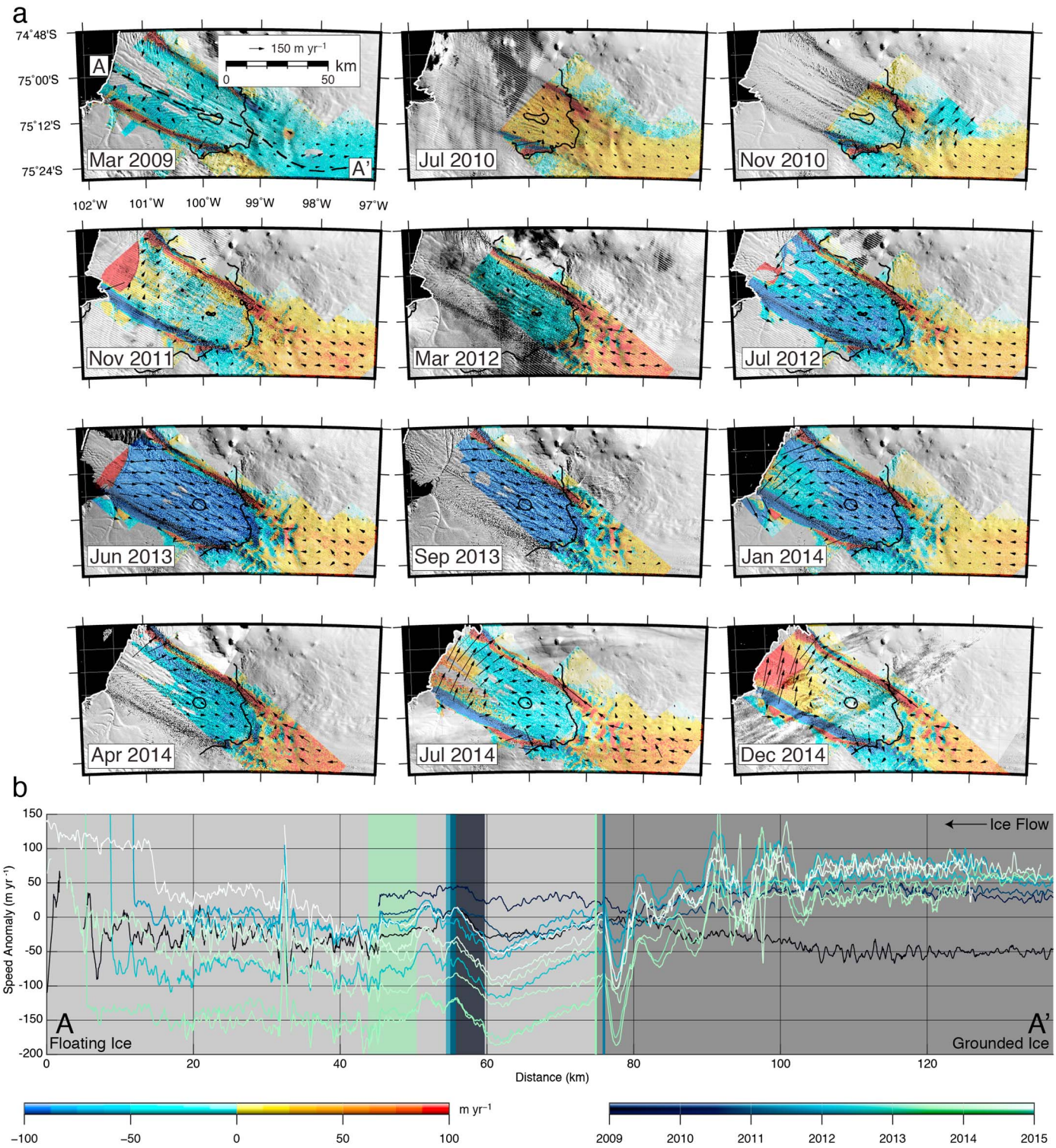

Figure 3. Ice velocity anomaly time series (2009 to 2015). (a) Ice velocity anomaly (left color bar; relative to December 2009; see Figure S4) time series maps (labeled by center date of SAR scenes used to construct the ice velocity mosaic). Vectors indicate ice flow direction anomaly. Grounding lines and grounded "islands" from 2009 (panels 1–3), 2011 (panels 4–6), and 2013 (panels 7–12) are plotted. Ice fronts are shown in white. Profile A-A′ (dashed black line) is shown (Figure 3b). Background is Landsat imagery contemporaneous with SAR ice velocity data. (b) Ice speed anomaly time series along profile A-A′. Grounding lines (vertical lines) and tidally grounded islands (vertical bars) are plotted for 2009 (green, km ~75), 2011 (cyan, km ~76), and 2013 (dark blue, km ~76). Grounded ice (2013) is denoted by the darker gray shading.

insensitive to fit method, window length, and GPS site used (Figure S3). We applied a 3 day median filter to the final data shown in Figure 2a, which are from GPS site SOW2 (Figures S2 and S3), for display purposes.

2.2. Synthetic Aperture Radar Data

We calculated ice velocity from TerraSAR-X synthetic aperture radar (SAR) pairs using a speckle-tracking approach [*Joughin*, 2002; *Joughin et al*., 2003, 2010]. Pixel-by-pixel formal uncertainties calculated following the methods of *Joughin* [2002] are ~25 m yr^{-1} (<1%) or less, and our SAR-derived and GPS-derived speeds agree to within this uncertainty (≤25 m yr^{-1}). In Figure 3a, we selected the December 2009 ice velocity (Figure S4) as the reference scene from which to compute velocity anomalies because data in that scene are spatially extensive and ice speed increases smoothly along flow with no visible localized flow anomalies. To derive the 2009 and 2013 grounding lines (the 2011 grounding line is from *Rignot et al*. [2014]), we used differenced range offsets determined from speckle-tracking using pairs of TerraSAR-X images. A single image pair has both tidal and horizontal motion. Assuming the motion is constant between the two TerraSAR-X image pairs, we can cancel the common horizontal motion by differencing pairs of speckle-tracked range offsets and obtain an estimate of differential vertical motion associated with tidal flexing [*E. Rignot*, 1998; *Joughin et al*., 2010, 2016]. The grounding lines were hand digitized at the upstream end of the gradient in differenced range offsets. This procedure is similar to the way grounding lines are computed using interferometric phase [*Goldstein et al*., 1993], which measures the same quantity. In sections of the grounding line with little horizontal curvature, the upper limit of flexural displacement, a proxy for the grounding line, is located to within uncertainty of <1 km. In areas of high curvature, uncertainty can exceed 1 km.

2.3. Ocean Temperature Measurements

To add to previous austral summer shipborne observations of water properties [*Dutrieux et al*., 2014a], we aggregated two ocean moorings deployed within a kilometer of each other to provide a 5 year temperature record at depth near the Pine Island Glacier ice shelf front. Mooring BSR5 was deployed in February 2009, while mooring iSTAR9 was deployed in February 2012. Both were recovered in January 2014. Both moorings were instrumented at several discrete depths between 320 and 800 m depth with SeaBird temperature and pressure loggers, yielding six- and seven-instrument time series at instrument-dependent sampling rates varying from 5 min to 2 h. During the period of sampling overlap between the two mooring sites, the temperature records are consistent. In Figure 2a, a measure of the ocean heat content is obtained by interpolating in depth the temperature record at both sites and averaging between 450 and 750 m depth over a time span of one month (30 day moving averages). Heat content is calculated as $Q = \rho c_p (T - T_f)$, where ρ is the density of the ocean, c_p is the ocean heat capacity, T is the depth-interpolated temperature, and T_f is the in situ freezing temperature.

The thermocline is the zone of large vertical gradient of temperature in the water column separating the cold winter water (WW) from the underlying, warm circumpolar deep water (CDW). There is no unique definition of this zone [cf. *Dutrieux et al*., 2014a], but its upper and lower depths can be defined by breaks in the slope of the temperature profile or threshold variations from the WW and CDW characteristics. In the mooring record (Figure 2), the upper bound of the thermocline (i.e., departure from WW to CDW) varies from 250 to 550 m depth and the lower bound varies from 550 to 770 m depth. Most of the ice shelf bottom is at depths that are within the bounds of the thermocline where most temperature variability occurs (Figure 1b).

2.4. Basal-Melt Rate Measurements

A subice, upward directed acoustic altimeter was installed at the base of a borehole within 5 km of the GPS array [*Stanton et al*., 2013]. The altimeter functioned for several months in early 2013. Acoustic backscatter amplitude provides a range offset time series between the instrument and ice bottom over $O(10)$ cm^2 area, with a sampling period of approximately 3 h. Range offsets are converted to basal-melt rate (Figure 2a) by taking the time derivative in a 15 day moving boxcar window using a linear fit. The first five days of data are eliminated, as they were biased by settling of the instrument relative to the ice bottom after hot-water drilling concluded [*Stanton et al*., 2013].

3. Results

3.1. Ice Velocity

Earlier results show that the glacier accelerated to a peak speed of ~4000 m yr^{-1} near the grounding line by 2009 [*Joughin et al*., 2010]. Speed remained nearly constant until early 2012 (black bars in Figure 2, panels 1–5 in Figure 3a, and Figure 3b). Through 2012 and until mid-2013, the overall speed decreased to ~3850 m yr^{-1} (black curve in Figure 2). Speed then increased again, reaching 3975 m yr^{-1} by early 2014 (Figure 2a) and returning to or above its approximate preslowdown speed in late 2014 (Figures 2a and 3). This is the only slowdown observed in at least the last two decades. The slowdown occurred across the well-imaged (central fast flowing) portion of the ice shelf and extended 10 km inland but was lower amplitude (~1%) and had little influence farther upstream (Figure 3 and Movie S1). The SAR data show that the ice shelf speedup continued into 2015, with the proximal grounded ice stream returning to its earlier (pre-2012) baseline speed.

3.2. Ocean Temperature

Mooring observations (2009–2014) indicate a seasonal cycle at the ice shelf front in the thickness of the underlying, warm CDW (0.5° to 1.2°C; Figures 2 and S1), at depths below 450 m, and of overlying, cold WW (−1.9° to − 1.5°C), with a November–December minimum in water column temperature (Figure 2a). An interannual fluctuation is superimposed on this annual cycle. Near the beginning of 2009, temperatures in the lower thermocline depth range (450–770 m; Figure 2) averaged 0.75°C, decreasing to a minimum below − 0.5°C in late 2012, then rising above +0.5°C by the beginning of 2014. During this cold period, the cold surface water layer thickened, the thermocline deepened and the CDW layer thinned. At the anomaly peak (late 2012), ocean heat content near the ice shelf cavity was reduced by ~60% compared to 2009, based on mooring observations (450–770 m depth), which should have reduced basal melting of the ice shelf. For January–February 2012 (before the anomaly peak), ocean observation-based balance flux calculations at the ice shelf front already indicate a 53% reduction in melt, while numerical modeling of ocean circulation in the ice shelf cavity yields a 31 to 38% decrease, through coupled reduction of ocean temperature and circulation [*Dutrieux et al*., 2014a]. Although of short duration, basal altimeter measurements also indicate a link between basal-melt rate and ocean temperature near the ice front (Figure 2a).

3.3. Ice-Dynamic Response to Ocean Forcing and Loss of Buttressing

Ice flow velocity correlates well with ocean temperature lagged ~275 days ($r = 0.73$; computed using the high-frequency GPS-derived velocity data; see Figure 2a), consistent with colder water allowing the ice shelf to thicken, increasing drag. The lag is expected to be longer than the circulation timescale (30–60 days) [*Heimbach and Losch*, 2012], in order for reduced melting to allow enough thickening to increase drag. Although the SAR data are less well sampled in time, they also indicate that ice speed and ocean temperature are likely correlated. Additional evidence that changing side drag influences flow velocity comes from the response to a calving event that occurred during November 2013. As the iceberg (B31) drifted away from PIG, reducing the shelf area available to generate side drag, speed increased ~1%. The glacier calved at least six times between 1972 and 2015 with no obvious relation to ocean temperature [*MacGregor et al*., 2012]. The November 2013 calving likely was also not a direct response to ocean forcing, but the speedup from loss of this thinnest part of the ice shelf shows its responsiveness to changing buttressing and highlights the system's coupled nature.

4. Discussion

Ocean simulations and observations indicate that strong easterly wind anomalies at the continental-shelf break (as observed in 2011–2012) weaken CDW advection from the open ocean [*Thoma et al*., 2008; *Dutrieux et al*., 2014a]. The 2011–2012 wind anomaly was forced by an atmospheric teleconnection from the remote tropical Pacific by a La Niña event [*Dutrieux et al*., 2014a]. Regional sea-ice/ocean modeling also suggests that anomalous atmospheric heat fluxes during late 2012 increased sea-ice production and thus WW volume in Pine Island Bay [*St-Laurent et al*., 2015]. Although the relative contributions of local versus remote atmospheric forcing, and their interactions, are not known, both could have reduced ocean temperature in Pine Island Bay and probably contributed to the 2012–2014 cold-ocean anomaly.

The thickness of the PIG ice shelf is determined primarily by the balance between ice advection and basal melting [*Dutrieux et al*., 2013], as accumulation variability has only minor effects on PIG ice shelf thickness

[*Medley et al*., 2014]. Since a high amplitude (~500 m), transverse seafloor ridge beneath the ice shelf limits access of the deepest and warmest waters to the grounding line (Figures 1b and S5) [*Jenkins et al*., 2010; *Muto et al*., 2016], only waters above ~750 m depth reach the grounding line in the inner cavity, cause melting, and feed a buoyant return flow [*Jenkins*, 2011], affecting basal-melt rate, ice thickness, ice drag, and ice flow along the entire ice shelf. The observed middepth thermal variability is thus indicative of the range of ocean temperatures to which the PIG ice shelf base was exposed during the study period (Figure 2b).

Taken together, the glaciological and oceanographic data produce a consistent picture of ocean forcing and glacier response. Our detailed observations began when ocean temperature was high, and the ice was flowing and thinning rapidly, following a large and likely ongoing ungrounding event [*Joughin et al*., 2010; *Rignot et al*., 2014]. Subsequent ocean cooling decreased basal-melt rates, allowing advection of thicker ice farther downstream, thus favoring increased buttressing from increased localized grounding, possibly aided by increased side shear from the thicker ice. The ice shelf slowed in response, in turn slightly slowing the grounded ice stream, and this at least temporarily halted grounding line retreat. The simplest interpretation is that basal-melt rate is directly proportional to cavity ocean heat content and in turn modifies ice velocity through changing drag resulting from ice thickness changes. Because ice thickness also depends on continued melting and the past grounding line and flow history, the link between ocean temperature and ice velocity is modified by associated changes in ice shelf cavity geometry, dampening the expected response, which would explain the observations.

The evolution of the small region grounded across the transverse bathymetric ridge is particularly interesting (Figure 3). *Joughin et al*. [2016] provided a detailed analysis of the time evolution of grounding over this region. Here we present an interpretation of our observations that is consistent with their results. Ice shelf drafts are close to seafloor elevations in several locations (Figure 1b), but especially over this bathymetric ridge, so that changes in thickness of ice advected from upstream are likely to affect grounding in this location. From late 2009 to early 2012, the grounded zone near km 45–50 shrank greatly (compare November 2010 to November 2011 in Figure 3a and the green 2009 and cyan 2011 bands in Figure 3b; see panels 4–8 in Figure 2 of *Joughin et al*. [2016]) due to the large ongoing ungrounding event [*Joughin et al*., 2010; *Rignot et al*., 2014]. Grounding was subsequently established downstream on the higher topography of the ridge crest near km 55–60, probably beginning in early 2012 (panels 8–10 in Figure 2 of *Joughin et al*. [2016]) and clearly established in our data by June 2013 (Figure 3a; dark blue band in Figure 3b), coincident with the main slowdown and consistent with the cold-ocean anomaly allowing advection of thicker ice into the ridge. We suspect that the region of grounding established by June 2013 was subsequently reduced by increasing basal-melt rate (Figure 2a; panels 11–15 in Figure 2 of *Joughin et al*. [2016]), contributing to the small positive velocity anomaly seen just upstream of the grounding line in our December 2014 map (Figure 3a). Changes in grounding affect ice velocity not only directly by changing backstress but also indirectly by changing ocean circulation and basal melting, through opening or closing ocean passages (especially in areas with a shallow water column such as near the bathymetric ridge), with subsequent effects on ice thickness advecting from upglacier in this strongly coupled glacier-ocean system [*Joughin et al*., 2016]. Regrounding of ice on previously submerged bathymetric ridges can thus have widespread effects on ice flow.

5. Conclusions

During the last two decades, the grounding line of PIG retreated down the continental side of the large seafloor ridge (Figures 1 and S5), likely in response to thinning due to an intrusion of warm waters beneath the ice shelf [*Payne et al*., 2004; *Jenkins et al*., 2010; *Dutrieux et al*., 2014a]. Based on limited observations and our knowledge of atmospheric teleconnections [*Turner et al*., 2004; *Steig et al*., 2012; *Dutrieux et al*., 2014a], ocean temperature fluctuations similar to the one we have documented may have occurred during this retreat. However, because the bed slope favored marine ice sheet instability, the glacier was not stabilized by cold-ocean anomalies. Recently, the grounding line entered a rougher, more nearly horizontal area (Figure S5) [*Joughin et al*., 2010, 2016]. This configuration is more sensitive to oceanic variability and less sensitive to marine instability, because bed elevation does not decrease rapidly and monotonically inland of the grounding line. Nonetheless, the current depth of the grounding line is such that flow speed and ice discharge are well out of balance, so that strong thinning will continue within the basin unless the grounding

line retreats or advances to a shallower position. The grounding line retreated into the zone of more subdued bed slopes in 2009 and stabilized at least temporarily [*Joughin et al*., 2010, 2016]. Ice speed did not decrease until 2012 when the cold-water anomaly began. The slowdown was likely also partially a result of the advection of thicker ice onto the bathymetric ridge [*Joughin et al*., 2016]; the lower ocean heat content likely lowered basal-melt rate, allowing thicker ice to advect farther downstream. As the water in the cavity subsequently warmed, however, speeds increased to their precold anomaly rates, suggesting grounding line retreat will resume.

Simulations using a temporally static basal-melt rate indicate that an eventual stepped retreat is likely over the next several decades [*Joughin et al*., 2010]. Future ocean temperature fluctuations may cause similar speed and grounding line fluctuations, so that retreat pace on interannual to subdecadal timescales will depend on the interplay of grounding line position, glacial and seabed geometry, and ocean forcing [*Joughin et al*., 2010; *Jamieson et al*., 2012; *Parizek et al*., 2013]. Model projections do not generally include ocean temperature forcing on interannual timescales and thus the cumulative effects of ocean temperature fluctuations on ice flow are unclear. Our data suggest that persistently cold oceanic conditions may be needed to restore PIG to stability even with its grounding line in a relatively flat region, consistent with the sustained, decadal-scale retreat predicted in modeling studies [*Joughin et al*., 2010; *Favier et al*., 2014; *Seroussi et al*., 2014; *De Rydt and Gudmundsson*, 2016]. Thus, for PIG or other drainages with retrograde bed slopes, once unstable retreat has been triggered, reversing the long-term sea level contribution likely would require significant multidecadal shifts away from the climatic changes that initiated more rapid melting and ice flow.

Acknowledgments

The work was supported by National Aeronautics and Space Administration grants NNX16AM01G (K.C.), NNX12AB69G (K.C. and D. H.), and NNX15AH84G (B.P.); U.S. National Science Foundation grants PLR-0732869 (D.H. and M.B.), PLR-0732730 (M.T.), PLR-1443190 (B.P.), PLR-0632282 (S.J.), ANT-0732926 (T.S.), AGS-138832 (B.P. and R.A.) and ANT-0424589 (I.J., K.C., R.A., S.A., and B.P.); New York University Abu Dhabi Research Institute grant G1204 (D.H.); U.K. Natural Environment Research Council iSTAR program—grants NE/J005703/1 (K.H. and B.W.), NE/G001367/1 (A.J. and P.D.), and NE/J005746/1 (A.J., K.H., B.W., and P. D.), and South Korean Polar Research Institute grant KOPRI PP15020 (S.L. and T.K.). The U.S.-NSF POLENET project provided GPS base data. Logistical support was provided by the U.S. Air Force, 139th Expeditionary Airlift Squadron of the New York Air National Guard, Kenn Borek Air, and by many dedicated individuals working as part of the Antarctic Support Contract, managed by Raytheon Polar Services Company and Lockheed-Martin, and by the officers, scientists and crew of RV Araon, RV Nathaniel B. Palmer and RRS James Clark Ross. GPS data are archived with UNAVCO (www.unavco.org). Oceanographic data have been submitted to the NOAA National Centers for Environmental Information (https://www.nodc.noaa.gov/), British Oceanographic Data Centre (http://www.bodc.ac.uk/), and IEDA/MGDS Southern Ocean portal (http://www.marine-geo.org/index.php). SAR-derived ice velocity fields and grounding lines, and basal altimeter range data are freely available from the corresponding author.

References

Alley, K. E., T. A. Scambos, M. R. Siegfried, and H. A. Fricker (2016), Impacts of warm water on Antarctic ice shelf stability through basal channel formation, *Nat. Geosci.*, *9*, 290–293, doi:10.1038/ngeo2675.

Alley, R. B., S. Anandakrishnan, K. Christianson, H. J. Horgan, A. Muto, B. R. Parizek, D. Pollard, and R. T. Walker (2015), Oceanic forcing of ice-sheet retreat: West Antarctica and more, *Annu. Rev. Earth Planet. Sci.*, *43*, 207–231, doi:10.1146/annurev-earth-060614-105344.

Chen, G. (1998), GPS kinematics positioning for airborne laser altimetry at Long Valley, PhD thesis, Mass. Inst. of Technol., Cambridge.

Cornford, S. L., et al. (2015), Century-scale simulations of the response of the West Antarctic Ice Sheet to warming climate, *Cryosphere*, *9*, 1579–1600, doi:10.5194/tc-9-1579-2015.

DeConto, R. M., and D. M. Pollard (2016), Contribution of Antarctica to past and future sea-level rise, *Nature*, *531*, 591–597, doi:10.1039/nature17145.

De Rydt, J., and G. H. Gudmundsson (2016), Coupled ice shelf-ocean modeling and complex grounding line retreat from a seabed ridge, *J. Geophys. Res. Earth Surf.*, *121*, 865–880, doi:10.1002/2015JF003791.

Dutrieux, P., D. G. Vaughan, H. F. J. Corr, A. Jenkins, P. R. Holland, I. Joughin, and A. H. Fleming (2013), Pine Island glacier ice shelf melt distributed at kilometer scale, *Cryosphere*, *7*, 1543–1555, doi:10.5194/tc-7-1543-2013.

Dutrieux, P., J. De Rydt, A. Jenkins, P. R. Holland, H. K. Ha, S. H. Lee, E. J. Steig, Q. Ding, E. P. Abrahamsen, and M. Schröder (2014a), Strong sensitivity of Pine Island ice-shelf melting to climatic variability, *Science*, *343*, 174–178, doi:10.1126/science.1244341.

Dutriuex, P., C. Stewart, A. Jenkins, K. W. Nicholls, H. F. J. Corr, E. Rignot, and K. Steffen (2014b), Basal terraces on melting ice shelves, *Geophys. Res. Lett.*, *41*, 5506–5513, doi:10.1002/2014GL060618.

Favier, L., G. Durand, S. L. Cornford, G. H. Gudmundsson, O. Gagliardini, F. Fillet-Chaulet, T. Zwinger, A. J. Payne, and A. M. Le Brocq (2014), Retreat of Pine Island Glacier controlled by marine ice-sheet instability, *Nat. Clim. Change*, *4*, 117–121, doi:10.1038/nclimate2094.

Heimbach, P., and M. Losch (2012), Adjoint sensitivities of sub-ice-shelf melt rates to ocean circulation under the Pine Island Ice Shelf, West Antarctica, *Ann. Glaciol.*, *53*(60), 59–69, doi:10.3189/2012AoG60A025.

Haran, T., J. Bohlander, T. Scambos, T. Painter, and M. Fahnestock (2014), MODIS Mosaic of Antarctica 2008-2009 (MOA2009) Image Map, [MODIS Mosaic of Antarctica 2008-2009 (MOA2009) Image Map, Version 1], Natl. Snow and Ice Data Cent., Boulder, Colo., doi:10.7265/N5KP8037.

Goldstein, R. M., H. Engelhardt, B. Kamb, and R. M. Frolich (1993), Satellite radar interferometry for monitoring ice sheet motion: Application to an Antarctic ice stream, *Science*, *262*, 1525–1530.

Jacobs, S. S., H. H. Hellmer, and A. Jenkins (1996), Antarctic ice sheet melting in the Southeast Pacific, *Geophys. Res. Lett.*, *23*, 957–960, doi:10.1029/96GL00723.

Jacobs, S. S., A. Jenkins, C. F. Giulivi, and P. Dutrieux (2011), Stronger ocean circulation and increased melting under Pine Island Glacier ice shelf, *Nat. Geosci.*, *4*, 519–523, doi:10.1038/ngeo1188.

Jamieson, S. S. R., A. Vieli, S. J. Livingstone, C. Ó Cofaigh, C. Stokes, C.-D. Hillenbrand, and J. A. Dowdeswell (2012), Ice-stream stability on a reverse bed slope, *Nat. Geosci.*, *5*, 799–802, doi:10.1038/ngeo1600.

Jenkins, A. (2011), Convection-driven melting near the grounding lines of ice shelves and tidewater glaciers, *J. Phys. Ocean.*, *41*, 2279–2294, doi:10.1175/JPO-D-11-03.1.

Jenkins, A., P. Dutrieux, S. S. Jacobs, S. D. McPhail, J. R. Perrett, A. T. Webb, and D. White (2010), Observations beneath Pine Island Glacier in West Antarctica and implications for its retreat, *Nat. Geosci.*, *3*, 468–472, doi:10.1038/ngeo890.

Joughin, I. (2002), Ice-sheet velocity mapping: a combined inteferometric and speckle-tracking approach, *Ann. Glaciol.*, *34*, 195–201.

Joughin, I., E. Rignot, C. E. Rosanova, B. K. Lucchitta, and J. Bohlander (2003), Timing and recent accelerations of Pine Island Glacier, Antarctica, *Geophys. Res. Lett.*, *30*(13), 1706, doi:10.1029/2003GL017609.

Joughin, I., B. E. Smith, and D. M. Holland (2010), Sensitivity of 21st century sea level to ocean-induced thinning of Pine Island Glacier, Antarctica, *Geophys. Res. Lett.*, *37*, L20502, doi:10.1029/2003GL017609.

Joughin, I., B. E. Smith, and B. Medley (2014), Marine ice sheet collapse potentially under way for the Thwaites Glacier basin. West Antartica, *Science*, *344*, 735–738, doi:10.1126/science.1249055.

Joughin, I., D. E. Shean, B. E. Smith, and P. Dutrieux (2016), Grounding line variability and subglacial lake drainage on Pine Island Glacier, Antarctica, *Geophys. Res. Lett.*, *43*, 9093–9102, doi:10.1002/2016GL070259.

King, M. (2004), Instruments and methods: Rigourous GPS data-processing strategies for glaciological applications, *J. Glaciol.*, *50*(171), 601–607.

Krabill, W. B. (2014), IceBridge ATM L2 icessn elevation, slope, and roughness, Version 2 2009 Antarctica DC-8, Boulder, Colorado USA, NASA National Snow and Ice Data Center Distributed Active Archive Center, doi:10.5067/CPRXXK3F39RV.

Langley, K., A. von Deschwanden, J. Kohler, A. Sinisalo, K. Matsuoka, T. Hattermann, A. Humbert, O. A. Nøst, and E. Isaksson (2014), Complex network of channels beneath an Antarctic ice shelf, *Geophys. Res. Lett.*, *41*, 1209–1215, doi:10.1002/2013GL058947.

Leuschen, C., P. Gogineni, F. Rodriguez-Morales, J. Paden, and C. Allen (2010, updated 2015), IceBridge MCoRDS L2 ice thickness, 2009 Antarctica DC-8, NASA DAAC at the Natl. Snow and Ice Data Cent., Boulder, Colo., doi:10.5067/GDQ0CUCVTE2Q.

MacGregor, J. A., G. A. Catania, M. S. Markowski, and A. G. Andrews (2012), Widespread rifting and retreat of ice-shelf margins in the eastern Amundsen Sea Embayment between 1972 and 2011, *J. Glaciol.*, *58*(209), 458–466, doi:10.3189/2012JoG11J262.

Marsh, O., H. A. Fricker, M. R. Siegfried, K. Christianson, K. W. Nicholls, H. F. J. Corr, and G. Catania (2016), High basal melting forming a channel at the grounding line of Ross Ice Shelf, Antarctica, *Geophys. Res. Lett.*, *43*, 250–255, doi:10.1002/2015GL066612.

Medley, B., et al. (2014), Constraining the recent mass balance of Pine Island and Thwaites glaciers, West Antarctica, with airborne observations of snow accumulation, *Cryosphere*, *8*, 1375–1392, doi:10.5194/tc-8-1375-2014.

Mercer, J. H. (1968), Antarctic ice and Sangamon sea level, *Int. Assoc. Sci. Hydrol. Publ.*, *79*, 215–225.

Moratto, Z. M., M. J. Broxton, R. A. Beyer, M. Lundy, and K. Husmann (2010), Ames Stereo Pipeline, NASA's open source automated stereogrammetry software, paper presented at 41st Lunar and Planetary Science Conference.

Mouginot, J., E. Rignot, and B. Scheuchl (2014), Sustained increase in ice discharge from the Amundsen Sea Embayment, West Antarctica, from 1973 to 2013, *Geophys. Res. Lett.*, *41*, 1576–1584, doi:10.1002/2013GL059069.

Muto, A., L. E. Peters, K. Gohl, I. Sasgen, R. B. Alley, S. Anandakrishnan, and K. L. Riverman (2016), Subglacial bathymetry and sediment distribution beneath Pine Island Glacier ice shelf modeled using aerogravity and in situ geophysical data: New results, *Earth Planet. Sci. Lett.*, *433*, 63–75, doi:10.1016/j.epsl.2015.10.037.

Paolo, F. S., H. A. Fricker, and L. Padman (2015), Volume loss from Antarctic ice shelves is accelerating, *Science*, *348*, 327–331, doi:10.1126/science.aaa0940.

Parizek, B. R., et al. (2013), Dynamic (in)stability of Thwaites Glacier, West Antarctica, *J. Geophys. Res. Earth Surf.*, *118*, 638–655, doi:10.1002/jgrf.20044.

Payne, A. J., A. Viele, A. Shepherd, D. J. Wingham, and E. Rignot (2004), Recent dramatic thinning of largest West Antarctic ice stream triggered by oceans, *Geophys. Res. Lett.*, *31*, L23401, doi:10.1029/2004GL021284.

Press, W. H., S. A. Teukolsky, W. T. Vetterling, and B. P. Flannery (2007), *Numerical Recipes*, 3rd ed., Cambridge Univ. Press, Cambridge, U. K.

Pritchard, H. D., S. R. M. Ligtenberg, H. A. Fricker, D. G. Vaughan, M. R. van den Broeke, and L. Padman (2012), Antarctic ice-sheet loss driven by basal melting of ice shelves, *Nature*, *484*, 502–505, doi:10.1038/nature10968.

Rignot, E. (1998), Tidal motion, ice velocity and melt rate of Petermann Gletscher, Greenland, measured from radar interferometry, *J. Glaciol.*, *42*(142), 476–485.

Rignot, E. (2008), Changes in West Antarctic ice stream dynamics observed with ALOS PALSAR data, *Geophys. Res. Lett.*, *35*, L12505, doi:10.1029/2008GL033365.

Rignot, E., and K. Steffen (2008), Channelized bottom melting and stability of floating ice shelves, *Geophys. Res. Lett.*, *35*, L02503, doi:10.1029/2007GL031765.

Rignot, E., J. Mouginot, and B. Scheuchl (2011a), Ice flow of the Antarctic ice sheet, *Science*, *333*, 1427–1430, doi:10.1126/science.1208336.

Rignot, E., J. Mouginot, and B. Scheuchl (2011b), MEaSUREs InSAR-based Antarctica ice velocity [MEaSUREs InSAR-Based Antarctica Ice Velocity Map, Version 1], NASA DAAC and the Natl. Snow and Ice Data Cent., Boulder, Colo.

Rignot, E., J. Mouginot, M. Morlighem, H. Seroussi, and B. Scheuchl (2014), Widespread, rapid grounding line retreat of Pine Island, Thwaites, Smith, and Kohler glaciers, West Antarctica, *Geophys. Res. Lett.*, *41*, 3502–3509, doi:10.1002/2014GL060140.

Rignot, E. J. (1998), Fast recession of a West Antarctic glacier, *Science*, *281*, 549–551.

Schoof, C. (2007), Ice sheet grounding line dynamics: Steady states, stability, and hysteresis, *J. Geophys. Res.*, *112*, F03S28, doi:10.1029/2006JF000664.

Seroussi, H., M. Morlighem, E. Rignot, J. Mouginot, E. Larour, M. Schodlok, and A. Khazendar (2014), Sensitivity of Pine Island Glacier, West Antarctica, to climate forcing for the next 50 years, *Cryosphere*, *8*, 166–1710, doi:10.5194/tc-8-1699-2014.

Shean, D. E., O. Alexandrov, Z. M. Moratto, B. E. Smith, I. R. Joughin, C. Porter, and P. Morin (2016), An automated, open-source pipeline for mass production of digitial elevation models (DEMs) from very-high-resolution commercial stereo satellite imagery, *ISPRS J. Photogramm. Remote Sens.*, *116*, 101–117, doi:10.1016/j.isprsjprs.2016.03.012.

Stanton, T. P., W. J. Shaw, M. Truffer, H. F. J. Corr, L. E. Peters, K. L. Riverman, R. Bindschadler, D. M. Holland, and S. Anandakrishnan (2013), Channelized ice melting in the ocean boundary layer beneath Pine Island Glacier, *Science*, *341*, 1236–1239, doi:10.1126/science.1239373.

Steig, E. J., Q. Ding, D. S. Battisti, and A. Jenkins (2012), Tropical forcing of Circumpolar Deep Water inflow and outlet glacier thinning in Amundsen Sea Embayment, West Antarctica, *Ann. Glaciol.*, *53*(60), 19–28, doi:10.3189/2012AoG60A110.

St-Laurent, P., J. M. Klinck, and M. S. Dinniman (2015), Impact of local winter cooling on the melt of Pine Island Glacier, Antarctica, *J. Geophys. Res. Oceans*, *120*, 6718–6732, doi:10.1002/2015JC010709.

Thoma, M., A. Jenkins, D. Holland, and S. Jacobs (2008), Modelling circumpolar deep water intrusions on the Amundsen Sea continental shelf, Antarctica, *Geophys. Res. Lett.*, *35*, L18602, doi:10.1029/2008GL034939.

Turner, J., J. C. Comiso, G. J. Marshall, T. A. Lachlan-Cope, T. Bracegirdle, T. Maksym, M. P. Meredith, Z. Wang, and A. Orr (2004), Nonannular atmospheric circulation change induced by stratospheric ozone depletion and its role in the recent increase of Antarctic sea ice extent, *Geophys. Res. Lett.*, *36*, L08502, doi:10.1029/2009GL037524.

Weertman, J. (1974), Stability of the junction of an ice sheet and an ice shelf, *J. Glaciol.*, *13*(67), 3–13.